Full-Envelope Flight Control for a Multi-Rotor Cessna-182 eVTOL

Hao Yang
School of Engineering
University of Leicester
Email: hy153@le.ac.uk

Rafael Morales
School of Engineering
University of Leicester
Email: rmm23@le.ac.uk

Abstract—This paper considers the flight control for an electric Vertical Take-Off and Landing vehicle, whose configuration is based on the fixed-wing Cessna 182 mounted with additional 4 tilting rotors to provide helicopter flight characteristics. Consequently, 2 flight modes are identified for this vehicle: helicopter mode and airplane mode. For the purposes of simple tuning and easy implementation, we exploit Proportional-Integral-Derivative methods in each flight mode for the control law design. The transition between the 2 modes are controlled based on a feedforward gain scheduling technique, which is typical for tiltrotor configurations. The performances of the controllers are first examined on the simplified/linearised models before they are tested on the nonlinear one, which leads to increased confidence in practice. The simulation results show that the control outcome is successful, in the sense that the vehicle can stabilise and provide fast tracking in each mode. Moreover, no significant changes in the flight properties are observed during the transition period.

Symbol	Meaning
β	sideslip angle [rad]
$\delta_{a,e,r}$	aileron/elevator/rudder deflection angle [rad]
δ_{Ti}	tilt angle of propeller *i* [rad]
ω	angular rate vector [rad/s]
ϕ,θ,ψ	roll/pitch/yaw angle [rad]
$\mathbf{F}$	force vector [N]
g	gravity constant [m/s^2]
$\mathbf{M}$	moment vector [kg m^2/s^2]
p,q,r	roll/pitch/yaw rate [rad/s]
$\bar{q}$	dynamic pressure [N/m^2]
T_i	thrust provided by propeller *i* [N]
u,v,w	longitudinal, lateral and vertical speed [m/s]
$\mathbf{V}$	velocity vector [m/s]

I. Introduction

Research and development of novel rotorcraft vehicles is being invigorated due to the emerging of Urban and Regional Air Mobility transportation concepts. Two key characteristics for such new configurations are semi or fully electrically powered aircraft and Vertical and Take-off Landing (VTOL) capabilities. Vehicles with the combination of such characteristics are known as eVTOL, which are essential to meet stringent environmental requirements and access densely populated areas. Additional requirements for these new applications include low noise emissions and high reliability for public acceptance. Recently, much efforts have been developed for eVTOL vehicles, see for instance [1], [2], [3], [4]. Due to the complex configuration [5] and lack of detailed model information, the flight control task of such aircraft is challenging in the sense that: i) a wide range of flight conditions, including vertical taking off and landing, forward flying and transitions between them, needs to be taken into account; ii) robustness is deemed important to deal with unmodelled dynamics, so that high reliability and airworthiness can be ensured.

This work intends to develop a control law for an eVTOL vehicle based on the Cessna-182 aircraft, in which four tiltrotors and one cruise propeller are equipped. The flight control for such vehicle was studied in [1], where the nonlinear dynamic inversion (NDI) method [6] and incremental nonlinear dynamic inversion (INDI) [7] control design methods are used. These techniques can indeed offer very good performance levels under well-known conditions. In practice, however, flight aerodynamics are highly uncertain and the implementation of such controllers are deemed complicated, which could undermine this control strategy.

For this reason, we instead follow a more traditional approach (Proportional-Integral-Derivative method), where two *unique* sets of control laws are developed: i) the first one corresponds to the helicopter mode, in which the vehicle's attitudes, positions are regulated; ii) the other one is used for the airplane mode, where the aircraft's attitudes are controlled. It is worth noting that both control laws includes the control of the rate signals, thus the vehicle is able to follow specific rate command as well as position/attitude command, leading to more precise control results. The design of the aforementioned control laws are tuned based on a comprehensive set of linearised models, and validated on the nonlinear model to observe the performance. The benefits of using the PID method include simple tuning and easy implementation, with certain robustness provided by its integral action to account for the simplification of the model. Lastly, the transition between these 2 modes are controlled via DC gain scheduling method [8], [9], [10].

This paper is structured into 5 sections. Section II briefly introduces the considered vehicle model with the model simplification included. Section III designs the control laws for the 2 operation modes and the transition between these 2 modes, with the performance first investigated by using the simplified/linearised models. Section IV proceeds to present the simulations on the nonlinear model, which also include the results of the transition control and the whole flight envelope

test. This manuscript concludes with some final remarks in Section V.

II. Vehicle Model

A. Overview of the Model

Property	Value
Mass m	1201.8 kg
Mass inertia I_{xx}	1285.30 kg m^2
Mass inertia I_{yy}	1824.91 kg m^2
Mass inertia I_{zz}	2666.86 kg m^2
Wing area S	16.16 m^2
Wingspan b	10.97 m
Length l	7.67 m
Number of tilt-rotor	4
Number of cruise rotors	1

TABLE I: Aircraft model data [11].

The vehicle model and its key aerodynamic properties can be seen in Fig. 1 and Table I, with the motion variables explained in Fig. 2. The motion equations can be expressed in the following form as [12]:

$$\dot{\mathbf{V}} = \frac{1}{m}(\mathbf{F}_{\text{total}} - \boldsymbol{\omega} \times m\mathbf{V}) \tag{1}$$

and

$$\dot{\boldsymbol{\omega}} = \mathbf{I}^{-1}(\mathbf{M}_{\text{total}} - \boldsymbol{\omega} \times \mathbf{I}\boldsymbol{\omega}) \tag{2}$$

where $\mathbf{V} = \begin{bmatrix} u \\ v \\ w \end{bmatrix}$ is the velocity vector, $\boldsymbol{\omega} = \begin{bmatrix} p \\ q \\ r \end{bmatrix}$ is the angular rate vector, and $\mathbf{I}$ is the inertia matrix.

Fig. 1: VTOL vehicle model for controller design [1].

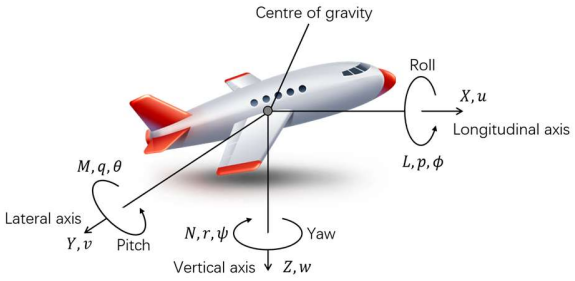

Fig. 2: Motion variable notations.

The total force vector $\mathbf{F}_{\text{total}} = \begin{bmatrix} X_{\text{total}} \\ Y_{\text{total}} \\ Z_{\text{total}} \end{bmatrix}$ and moment vector $\mathbf{M}_{\text{total}} = \begin{bmatrix} L_{\text{total}} \\ M_{\text{total}} \\ N_{\text{total}} \end{bmatrix}$ are comprised of aerodynamics, propulsion and gravity contributions [1]:

$$\mathbf{F}_{\text{total}} = \mathbf{F}_{\text{aero}} + \mathbf{F}_{\text{prop}} + \mathbf{F}_{\text{grav}} \tag{3}$$

$$\mathbf{M}_{\text{total}} = \mathbf{M}_{\text{aero}} + \mathbf{M}_{\text{prop}} \tag{4}$$

The aerodynamic contributions are defined by their dimensionless coefficients as follows:

$$\mathbf{F}_{\text{aero}} = \begin{bmatrix} C_X \\ C_Y \\ C_Z \end{bmatrix} \bar{q}S \tag{5}$$

$$\mathbf{M}_{\text{aero}} = \begin{bmatrix} bC_l \\ \bar{c}C_m \\ bC_n \end{bmatrix} \bar{q}S \tag{6}$$

The gravity contribution is expressed as:

$$\mathbf{F}_{\text{grav}} = \begin{bmatrix} X_{\text{grav}} \\ Y_{\text{grav}} \\ Z_{\text{grav}} \end{bmatrix} = \begin{bmatrix} -\sin\theta \\ \sin\phi\cos\theta \\ \cos\phi\cos\theta \end{bmatrix} mg \tag{7}$$

and the propulsion contributions are represented by:

$$\mathbf{F}_{\text{prop}} = \begin{bmatrix} X_{\text{prop}} \\ Y_{\text{prop}} \\ Z_{\text{prop}} \end{bmatrix} = \begin{bmatrix} \sum_{i=1}^{4} T_i \cos\delta_{T_i} \\ 0 \\ -\sum_{i=1}^{4} T_i \sin\delta_{T_i} \end{bmatrix} \tag{8}$$

$$\mathbf{M}_{\text{prop}} = \begin{bmatrix} L_{\text{prop}} \\ M_{\text{prop}} \\ N_{\text{prop}} \end{bmatrix} = \mathcal{M} \begin{bmatrix} T_1 \\ T_2 \\ T_3 \\ T_4 \end{bmatrix} \tag{9}$$

where M is described in Eq. (10), k_m is the torque constant of the propellers, dx_f, dy_f, dz_f and dx_r, dy_r, dz_r are the locations of the front and rear propellers, respectively, see Fig. 3.

By using the Aerospace Blockset, the above aerodynamic equations can be implemented in Simulink to build a 6 Degree-Of-Freedom (DOF) nonlinear model as shown in Fig. 4, where the control inputs are propeller thrust T_i, and aileron/elevator/rudder deflection angle $\delta_{a,e,r}$. The outputs of

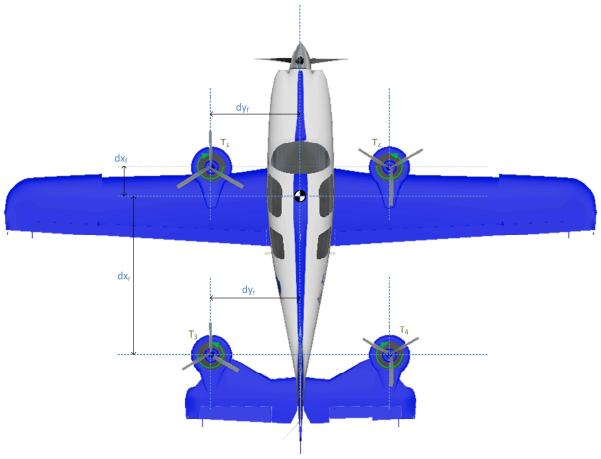

Fig. 3: Geometry information of the model [1].

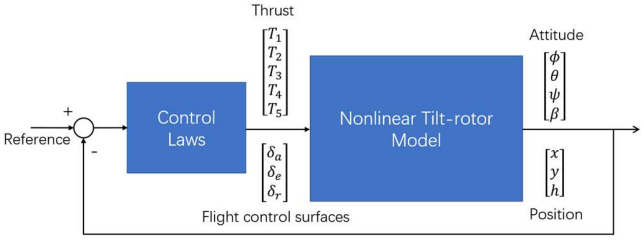

Fig. 4: Control diagram for the nonlinear tilt-rotor model.

interest are Euler rotation angles $\begin{bmatrix}\phi\\ \theta\\ \psi\end{bmatrix}$, sideslip angle β and position vector regarding the earth reference (inertial) frame $\begin{bmatrix}x\\ y\\ h\end{bmatrix}$, where $h = -z$ denotes the altitude of the vehicle.

B. Model Simplification

In order to carry out the control design task, it is standard to first obtain linear models by simplifying/linearising the nonlinear vehicle dynamics. With this aim, we first identify two basic modes for this vehicle: i) Helicopter mode, which refers to VTOL and hover flight conditions. These manoeuvres are manipulated through the thrust produced by the 4 tilting rotors

$$\mathcal{M} = \begin{bmatrix} dy_f \sin\delta_{T_1} - k_m \cos\delta_{T_1} & -dy_f \sin\delta_{T_2} + k_m \cos\delta_{T_2} \\ dx_f \sin\delta_{T_1} + dz_f \cos\delta_{T_1} & dx_f \sin\delta_{T_2} + dz_f \cos\delta_{T_2} \\ k_m \sin\delta_{T_1} + dy_f \cos\delta_{T_1} & -k_m \sin\delta_{T_2} - dy_f \cos\delta_{T_2} \end{bmatrix}$$

$$\begin{bmatrix} dy_r \sin\delta_{T_3} + k_m \cos\delta_{T_3} & -dy_r \sin\delta_{T_4} - k_m \cos\delta_{T_4} \\ -dx_r \sin\delta_{T_3} - dz_r \cos\delta_{T_3} & -dx_r \sin\delta_{T_4} - dz_r \cos\delta_{T_4} \\ -k_m \sin\delta_{T_3} + dy_r \cos\delta_{T_3} & k_m \sin\delta_{T_4} - dy_r \cos\delta_{T_4} \end{bmatrix} \quad (10)$$

($T_1 \sim T_4$), hence the aircraft behaves like a quad-rotor vehicle. ii) Airplane mode, on the other hand, corresponds to fixed-wing flight operation and the flight properties are controlled via the control surfaces ($\delta_{a,e,r}$), while the front propeller thrust T_5 is assumed to be at its maximum power setting. The model simplification for each mode is discussed in detail as follows.

1) Helicopter Mode: In this mode, we follow the standard dynamics simplification procedures for quad-rotor vehicles, see for example [13], [14], [15], [16]. By assuming that the angular rate vector ω is very small and hence negligible during the VTOL and hover, Eq. (1) and Eq. (2) can be simplified as:

$$\begin{bmatrix}\dot{u}\\ \dot{v}\\ \dot{w}\end{bmatrix} = \frac{1}{m}\begin{bmatrix}X_{\text{total}}\\ Y_{\text{total}}\\ Z_{\text{total}}\end{bmatrix} \quad (11)$$

and

$$\begin{bmatrix}\dot{p}\\ \dot{q}\\ \dot{r}\end{bmatrix} = \begin{bmatrix}I_{xx}^{-1} & 0 & 0\\ 0 & I_{yy}^{-1} & 0\\ 0 & 0 & I_{zz}^{-1}\end{bmatrix}\begin{bmatrix}L_{\text{total}}\\ M_{\text{total}}\\ N_{\text{total}}\end{bmatrix} \quad (12)$$

respectively. It is well known that the relationship between the inertia axis Euler angles (ϕ,θ,ψ) and body-fixed axis angular rates (p,q,r) is represented by:

$$\begin{bmatrix}\dot{\phi}\\ \dot{\theta}\\ \dot{\psi}\end{bmatrix} = \begin{bmatrix}1 & \sin\phi\tan\theta & \cos\phi\tan\theta\\ 0 & \cos\phi & -\sin\theta\\ 0 & \sin\phi\sec\theta & \cos\phi\sec\theta\end{bmatrix}\begin{bmatrix}p\\ q\\ r\end{bmatrix} \quad (13)$$

By assuming that the vehicle perturbations are small, we can treat ϕ,θ,ψ as small angles, then Eq. (13) can be approximated as:

$$\begin{bmatrix}\dot{\phi}\\ \dot{\theta}\\ \dot{\psi}\end{bmatrix} = \begin{bmatrix}p\\ q\\ r\end{bmatrix} \quad (14)$$

which yields to

$$\begin{bmatrix}\ddot{\phi}\\ \ddot{\theta}\\ \ddot{\psi}\end{bmatrix} = \begin{bmatrix}I_{xx}^{-1} & 0 & 0\\ 0 & I_{yy}^{-1} & 0\\ 0 & 0 & I_{zz}^{-1}\end{bmatrix}\begin{bmatrix}L_{\text{total}}\\ M_{\text{total}}\\ N_{\text{total}}\end{bmatrix}$$

Moreover, notice that the aerodynamic contribution in $\mathbf{M}_{\text{total}}$ is insignificant in the helicopter mode, thus the above equation can be further simplified to:

$$\begin{bmatrix}\ddot{\phi}\\ \ddot{\theta}\\ \ddot{\psi}\end{bmatrix} = \begin{bmatrix}I_{xx}^{-1} & 0 & 0\\ 0 & I_{yy}^{-1} & 0\\ 0 & 0 & I_{zz}^{-1}\end{bmatrix}\mathcal{M}\begin{bmatrix}T_1\\ T_2\\ T_3\\ T_4\end{bmatrix} \quad (15)$$

where in the helicopter mode, $\mathcal{M}$ becomes:

$$\mathcal{M} = \begin{bmatrix} dy_f & -dy_f & dy_r & -dy_r \\ dx_f & dx_f & -dx_r & -dx_r \\ k_m & -k_m & -k_m & k_m \end{bmatrix}$$

It remains to derive a linear relationship between the thrusts and the vehicle position. Similarly, the velocity vector (bodyfixed axis frame) and the position of the vehicle (inertial axis frame) can be related such that:

$$\begin{bmatrix}\dot{x}\\ \dot{y}\\ \dot{z}\end{bmatrix} = \mathbf{D}^T\begin{bmatrix}u\\ v\\ w\end{bmatrix} \quad (16)$$

where **D** is the direction cosine matrix [12] defined as:

$$= \begin{bmatrix} \cos\theta\cos\psi & \cos\theta\sin\psi & -\sin\theta \\ \sin\phi\sin\theta\cos\psi & \sin\phi\sin\theta\sin\psi & \sin\phi\cos\theta \\ -\cos\phi\sin\psi & +\cos\phi\cos\psi & \\ \cos\phi\sin\theta\cos\psi & \cos\phi\sin\theta\sin\psi & \cos\phi\cos\theta \\ +\sin\phi\sin\psi & -\sin\phi\cos\psi & \end{bmatrix}$$

D

By combining Eq. (11) and Eq. (16), the dynamical model of the quad-rotor in terms of positions can be described by the following equations:

$$\begin{cases} \ddot{x} = -\frac{1}{m}(\cos\phi\sin\theta\cos\psi + \sin\phi\sin\psi)\sum_{i=1}^{4} T_i \\ \ddot{y} = -\frac{1}{m}(\cos\phi\sin\theta\sin\psi - \sin\phi\cos\psi)\sum_{i=1}^{4} T_i \\ \ddot{h} = \frac{1}{m}(\cos\phi\cos\theta)\sum_{i=1}^{4} T_i - g \end{cases} \quad (17)$$

Note that the aerodynamics contribution in the force vector is also negligible, so that it is excluded in the above equations. Typically, the yaw angle is not used for the position control in the quad-rotor [17], [18], hence Eq. (17) can be further simplified by assuming ψ is relatively small such that:

$$\begin{cases} \ddot{x} = -\frac{1}{m}(\cos\phi\sin\theta)\sum_{i=1}^{4} T_i \\ \ddot{y} = \frac{1}{m}\sin\phi\sum_{i=1}^{4} T_i \\ \ddot{h} = \frac{1}{m}(\cos\phi\cos\theta)\sum_{i=1}^{4} T_i - g \end{cases} \quad (18)$$

Therefore, the simplified model in the helicopter mode is summarised in the following:

$$\begin{cases} \frac{m\ddot{h}+mg}{\cos\phi\cos\theta} = \sum_{i=1}^{4} T_i \\ \ddot{\phi} = I_{xx}^{-1} L_{\text{total}} \\ \ddot{\theta} = I_{yy}^{-1} M_{\text{total}} \\ \ddot{\psi} = I_{zz}^{-1} N_{\text{total}} \end{cases} \quad (19)$$

and

$$\begin{cases} \frac{m\ddot{x}}{-\cos\phi\sum_{i=1}^{4} T_i} = \sin\theta \\ \frac{m\ddot{y}}{\sum_{i=1}^{4} T_i} = \sin\phi \end{cases} \quad (20)$$

where Eq. (19) can be equivalently represented in the matrix form as:

$$\begin{bmatrix} \frac{m\ddot{h}+mg}{\cos\phi\cos\theta} \\ \ddot{\phi} \\ \ddot{\theta} \\ \ddot{\psi} \end{bmatrix} = \begin{bmatrix} 1 & 0 & 0 & 0 \\ 0 & I_{xx}^{-1} & 0 & 0 \\ 0 & 0 & I_{yy}^{-1} & 0 \\ 0 & 0 & 0 & I_{zz}^{-1} \end{bmatrix} \begin{bmatrix} \sum_{i=1}^{4} T_i \\ L_{\text{total}} \\ M_{\text{total}} \\ N_{\text{total}} \end{bmatrix}$$

Vehicle mode	Control method	Inputs used	Controlled outputs
Helicopter	PID		$, \theta, \psi]^T$, $[x, y, h]^T$
Airplane	PID		$[\phi, \theta, \beta]^T$
Transition	gain scheduling		-

TABLE II: Control strategy for different modes. and

it is easy to find out that

$$\begin{bmatrix} \sum_{i=1}^{4} T_i \\ L_{\text{total}} \\ M_{\text{total}} \\ N_{\text{total}} \end{bmatrix} = \mathcal{M}_{\text{new}} \begin{bmatrix} T_1 \\ T_2 \\ T_3 \\ T_4 \end{bmatrix}$$

where

$$\mathcal{M}_{\text{new}} = \begin{bmatrix} 1 & 1 & 1 & 1 \\ dy_f & -dy_f & dy_r & -dy_r \\ dx_f & dx_f & -dx_r & -dx_r \\ k_m & -k_m & -k_m & k_m \end{bmatrix}$$

Finally, the engine dynamics for thrust per rotor is modelled as [1], [2]:

$$\frac{T_i(s)}{T_{i_{\text{comm}}}(s)} = \frac{3}{s+3}, \forall i = 1, \ldots, 4 \quad (21)$$

We observe from the simplified model (Eq. (19)- (20)) that the vehicle dynamics in the helicopter mode is decoupled for the attitude angles and positions, which is governed by double integrators in addition to the engine dynamics (Eq. (21)).

2) Airplane Mode: The linearisation in this mode is carried out by first trimming the vehicle at the cruise condition (70 m/s forward speed, 300 m altitude), then by using the System Identification Toolbox provided in MATLAB, the following 3 linearised systems are identified:

$$\begin{cases} G_\theta(s) = \frac{\theta(s)}{\delta_e(s)} = \frac{-192.5s^2 - 22.35s - 9.235}{s^4 + 45.35s^3 + 110.5s^2 + 10.31s + 4.406} \\ G_\phi(s) = \frac{\phi(s)}{\delta_a(s)} = \frac{80.8s^2 + 113.9s + 698.2}{s^4 + 14.45s^3 + 18.81s^2 + 137.6s + 7.537} \\ G_\beta(s) = \frac{\beta(s)}{\delta_r(s)} = \frac{9.154s^2 + 145.3s + 2.869}{s^4 + 14.45s^3 + 18.81s^2 + 137.6s + 7.537} \end{cases} \quad (22)$$

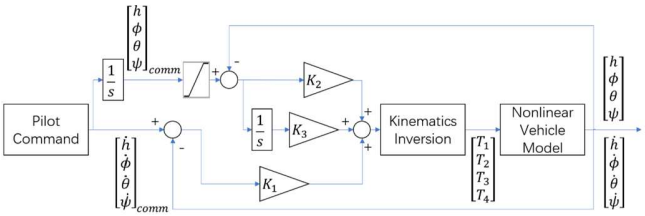

Fig. 5: Attitude and height control diagram in the helicopter mode.

	K_1	K_2	K_3
height	1.1	0.3	0.01
roll	9	1900	0.7
pitch	16	2500	1
yaw	21	3700	1.6
longitudinal	0.8	0.001	10^{-5}
lateral	0.8	0.001	10^{-5}

TABLE III: Control gains in the helicopter mode.

A. Helicopter Mode

The first part of control law design focuses on the helicopter mode, which accounts for vertical take-off, hover and vertical landing flight condition. In this mode, the front propeller is disabled ($T_5 = 0$), and the aircraft flight control surfaces ($\delta_{a,e,r}$) are also not used. As a consequence, the vehicle behaves like a quad-rotor and its positions and attitudes are controlled only by the thrust of the 4 tilt-rotors.

1) Attitude and Height Control: The control diagram for height and attitudes is shown in Fig. 5, where the rate commands are generated by the pilot, and the gain K_1 is used to regulate the vehicle to follow these rate signals. An integrator is used to transform the rates into height and attitude commands, in which the gain K
between these commands and the actual responses. In addition, an integral action is added in such difference with the gain K_3 in order to achieve some robustness associated with model mismatch. Note that the rate commands are set to 0 when the integrator reaches the saturation limits (desired values).

The 3 gains for attitude and height control are specified in Table III, and they are tuned based on the simplified plants described previously in Eq. (19):

2 is used for the difference

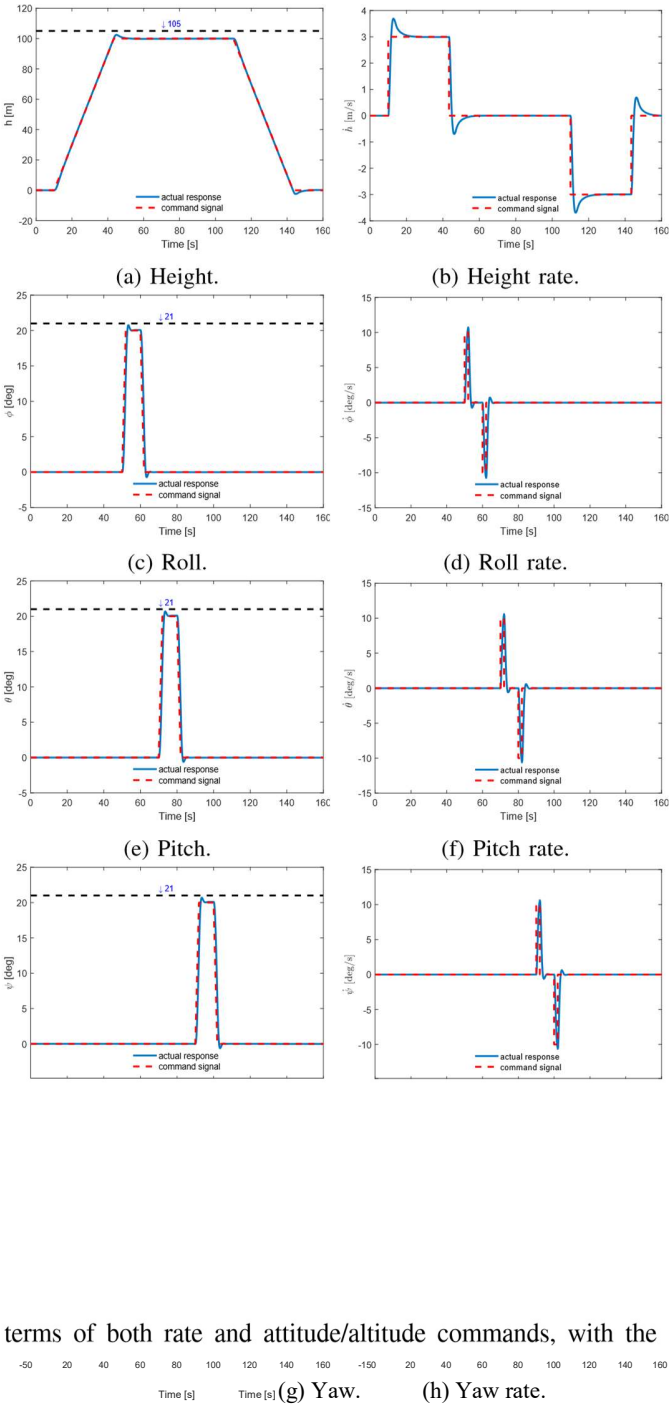

(a) Height. (b) Height rate.
(c) Roll. (d) Roll rate.
(e) Pitch. (f) Pitch rate.
(g) Yaw. (h) Yaw rate.

Fig. 6: Linear simulation results for attitude and height control (helicopter mode).

terms of both rate and attitude/altitude commands, with the

III. Full Envelope Control Law Design

The control strategy for each operation condition is illustrated in Table II, where in both operation modes, the control laws are constructed by simple-to-tune ProportionalIntegral-Derivative (PID) method. The transition

the designed control law is able to provide fast tracking in between these 2 modes are controlled based on DC gain scheduling, which is a popular method and has been widely employed in many applications, see [8], [9], [10]. Detailed descriptions of the control strategy in each flight mode are listed below.

$$\begin{cases} G_h(s) = \dfrac{3}{s^2(s+3)} \\ G_\phi(s) = \dfrac{3I_{xx}^{-1}}{s^2(s+3)} \\ G_\theta(s) = \dfrac{3I_{yy}^{-1}}{s^2(s+3)} \\ G_\psi(s) = \dfrac{3I_{zz}^{-1}}{s^2(s+3)} \end{cases} \quad (23)$$

In order to examine the control performance, we perform the simulations on the simplified systems shown in Eq. (23). The results can be seen from Fig. 6, where we observe that overshoot in terms of the height and attitude responses being less than 5%.

2) Longitudinal and Lateral Position Control: The positions regarding x and y are controlled by changing the pitch and roll angle, see Fig. 7. The pilot commands are similarly assumed to

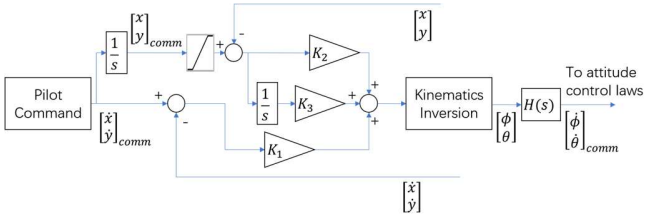

be rate signals, and in order to generate rate commands $\dot{\phi}$ and $\dot{\theta}$ for the pitch and roll control laws designed previously, the following transfer function is used:

$$H(s) = \frac{s}{0.1s+1}$$

Such high-pass filter is commonly used in Simulink in order to replace the Derivative Block.

Fig. 7: Longitudinal and lateral position control diagram.

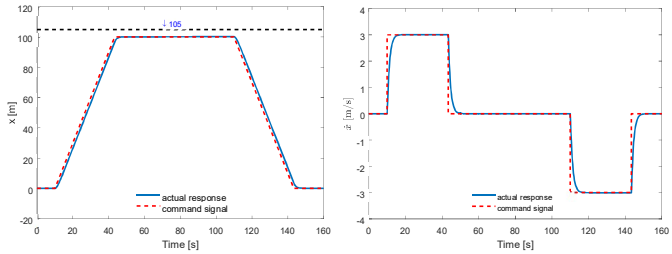

(a) Longitudinal position. (b) Longitudinal rate.

Fig. 8: Linear simulation results for x and y position control (helicopter mode).

It is shown in Eq. (20) that the dynamics regarding x and y can be represented by a double integrator:

$$G_{x,y}(s) = \frac{1}{s^2}$$

and the control law is similarly tuned by using the simplified plant shown above, where the 3 gains are listed in Table III. The linear performances are examined in Fig. 8, in which we notice that there is no observable overshoot, and the tracking performance is also very good. It is noted that since the simplified plants in terms of x and y positions are identical, only one set of the simulation results is shown in Fig. 8.

	K_1	K_2	K_3
roll	0.6	42	2
pitch	-0.6	-31	-1.6
sideslip	1.9	21	0.6

B. Airplane Mode Control

This mode corresponds to the standard fixed wing flight operation, where the 4 tilt-rotors are switched off ($T_{1\text{-}4} = 0$), the front propeller is assumed to be at the maximum thrust and the flight properties are controlled by the control surfaces ($\delta_{a/e/r}$). We adopt the same control law used previously, in which 3 gains are used to regulate both rates and attitudes, see Fig. 9. The 3 gains K_1, K_2 and K_3 are tuned according to the linearised plants

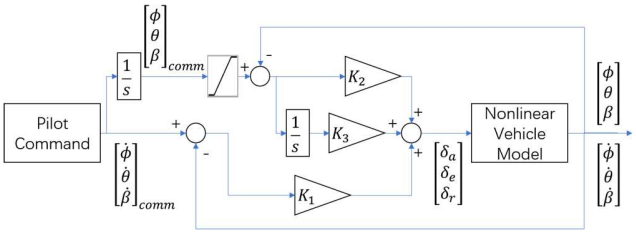

in Eq. (22), and their values are shown in Table IV. Linear simulation results are presented in Fig. 10, and it is clear that the control law provides very good performance for roll and pitch attitudes, in which fast tracking in terms of both rate and attitude commands are achieved without overshoots. The performance regarding the sideslip control is less satisfactory, in the sense that about 8% steadystate error and damping in the rate response are observed.

C. Transition Control

As described earlier, the transition between the two operation conditions are controlled via DC gain scheduling, whose general idea is described in Fig. 11. The control weight W Fig. 9: Airplane mode control diagram.

TABLE IV: Control gains in the airplane mode.

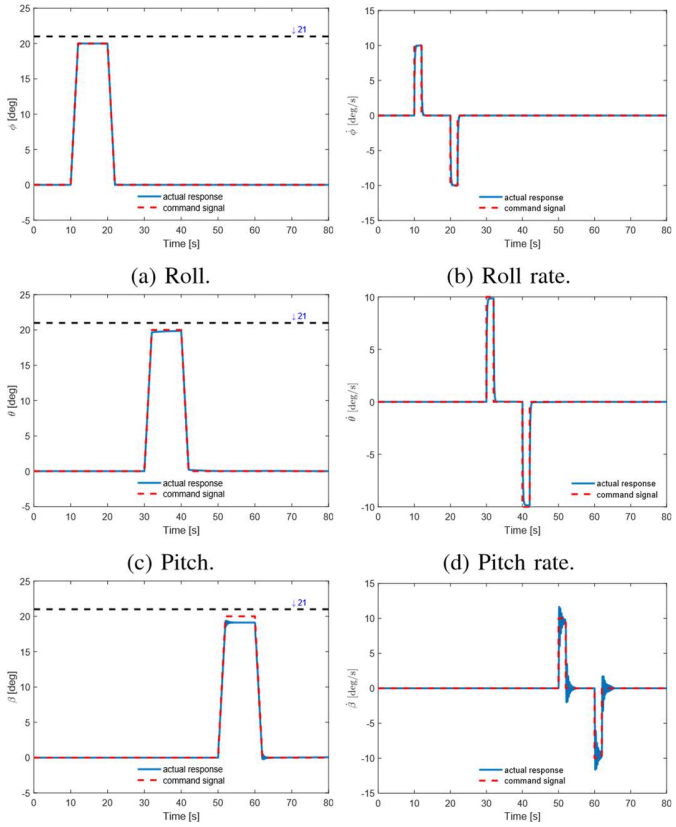

(a) Roll. (b) Roll rate.

(c) Pitch. (d) Pitch rate.

(e) Sideslip. (f) Sideslip rate.

Fig. 10: Linear simulation results (airplane mode).

depends on the rotor tilt angles δ_{Ti} and varies from 0 to 1. For simplicity, we assume that the 4 tilt angles are identical during the transition period, then the algorithm regarding W can be represented as follows:

$$W = \begin{cases} 1, & \delta_T \geq 75^\circ \\ 1 - \dfrac{75 - \delta_T}{25}, & 50^\circ \leq \delta_T < 75^\circ \\ 0, & \delta_T < 50^\circ \end{cases} \tag{24}$$

B. Airplane Mode

We continue to investigate the airplane mode controller performance on the nonlinear model, see Fig. 15. Note that the simulation is performed at the trimmed flight condition, so that the measurements regarding the 3 angles are expressed as the difference from the trimmed positions. Compared to the linear results shown in Fig. 10, it is noted that the sideslip controller performs slightly better on the nonlinear model, in which less steady-state error is observed. On the other hand, the roll and pitch controllers can provide very good performance in terms of command tracking, which is similar to the results shown in the linear simulations. It is worth noting that only minor cross coupling effects are observed between the 3 angles and their rates, indicating that the dynamics is well decoupled. Finally, the deflection angles of the aileron, elevator and rudder in this simulation are shown in Fig. 16, where the control actions are within reasonable ranges.

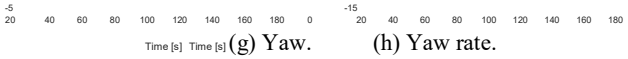

(g) Yaw. (h) Yaw rate.

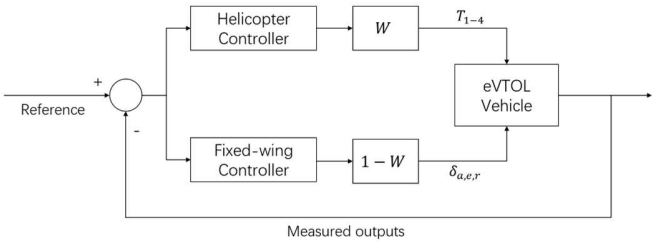

Fig. 11: DC gain scheduling structure for transition control.

IV. Simulation Results

In this section, we proceed to perform the simulations on the nonlinear vehicle model, and detailed results are presented below.

A. Helicopter Mode

The designed control laws are first examined in the helicopter mode in terms of attitude and height control, where the results are shown in Fig. 12. It is clearly seen that the performances are very similar to those of the linear simulations in Fig. 6, in the sense that the vehicle can quickly follow the height and attitude commands as well as their rate commands with minor overshoots. It is worth noting that the aircraft is able to hold the altitude while performing the roll, pitch and yaw manoeuvres, indicating that there are limited couplings from the three angles on the height control.

We then test the longitudinal and lateral position control laws on the nonlinear model, and the results can be seen in Fig. 13, where the longitudinal and lateral rate commands $\dot{x}, \dot{y}$ are engaged when the vehicle reaches 100 m altitude. We observe that the two controllers provide fast tracking and the vehicle is also able to maintain its altitude level during the longitudinal and lateral movements.

Finally, the power consumption for these two simulations are presented in Fig. 14, and it is clear that they are within the maximum range.

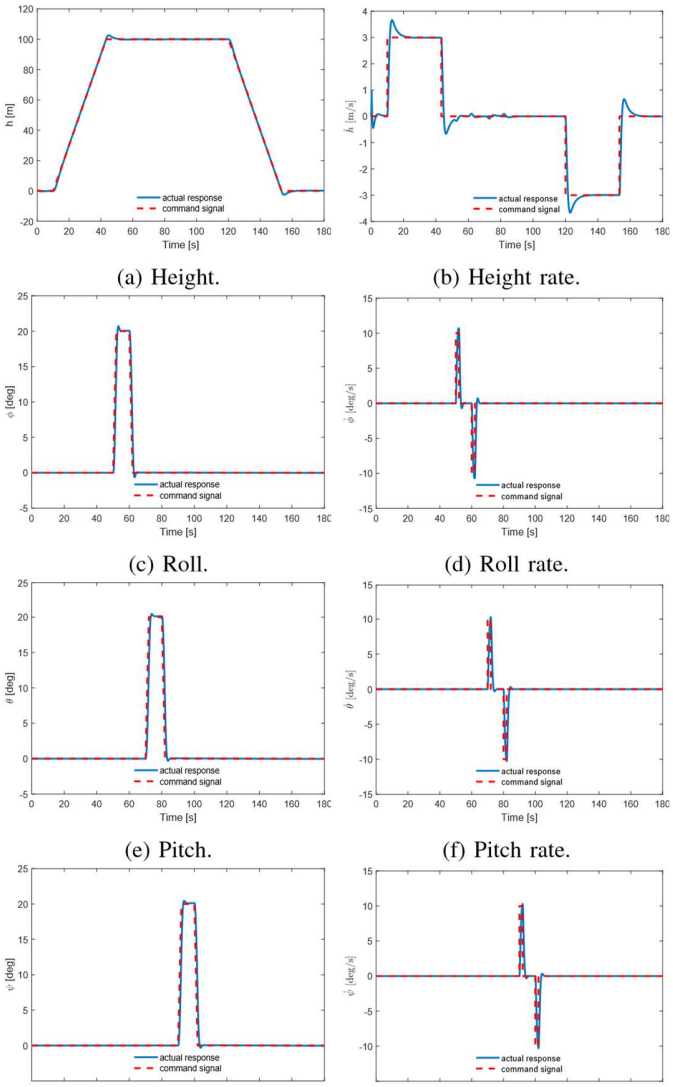

(a) Height. (b) Height rate.

(c) Roll. (d) Roll rate.

(e) Pitch. (f) Pitch rate.

Fig. 12: Nonlinear simulation results for attitude and height control (helicopter mode).

C. Whole Flight Test

The proposed control law is further tested in the whole flight condition, which includes the transition between the 2 operation modes. In the following simulation, the final destination is set as $x = 30$ km and $y = 8$ km. The vehicle first takes off vertically to the altitude $h = 300$ m, and the first transition (helicopter to airplane) occurs at $t = 400$ s, in which the conversion rate of the tilt rotor is 6 deg/s, leading to 15 s transition period. In addition, the front propeller (T_5) is activated 10 s earlier, so that the a certain forward speed is obtained before the first transition. The vehicle then cruises forward at 300 m altitude level, where the trimmed pitch position is $\theta_{trim} = -15^\circ$. In order to change the vehicle's heading, a 20 deg turn is executed at $t = 550$ s. The second

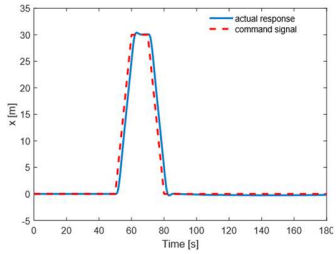

(a) Longitudinal position.

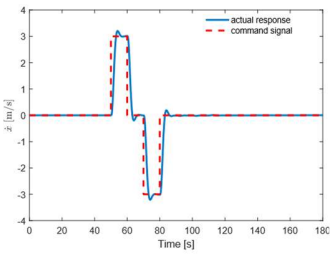

(b) Longitudinal position rate.

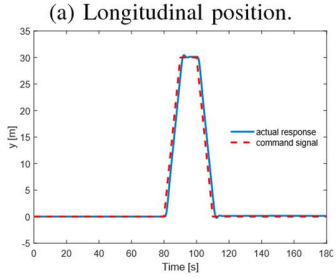

(c) Lateral position.

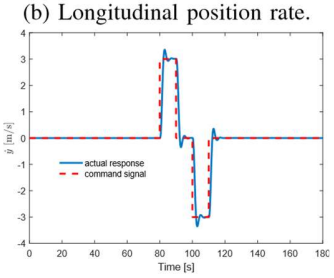

(d) Lateral position rate.

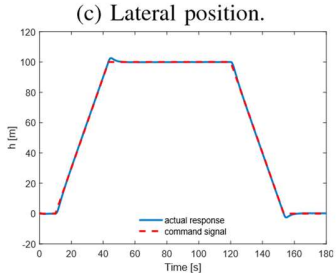

(e) Height.

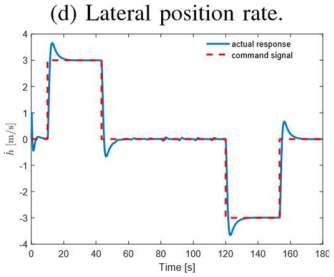

(f) Height rate.

Fig. 13: Nonlinear simulation results for longitudinal and lateral position control (helicopter mode).

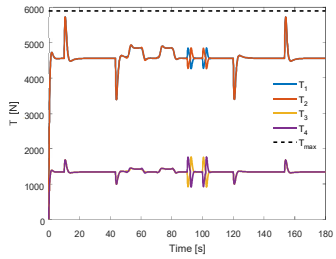

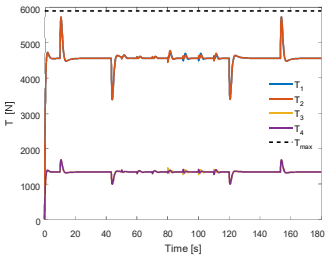

(a) Power consumption for attitude and height control.

(b) Power consumption for longitudinal and lateral position control.

Fig. 14: Power consumption.

transition (airplane to helicopter) starts when the vehicle is close to the destination, and the conversion rate is also set as 6 deg/s. The front propeller (T_5) is switched off at the end of the second transition, then the vehicle gradually approaches to the final destination and performs vertical landing. The flight path is presented in Fig. 17, and the simulation results are shown in Fig. 18. It is clear that the proposed gain scheduling method is able to stabilise the vehicle during both transition periods, in which the flight properties vary in acceptable ranges. We observe that the aircraft successfully reaches the final destination, in which no large control actions

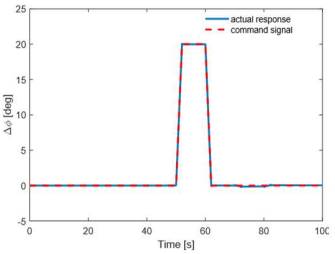

(a) Roll.

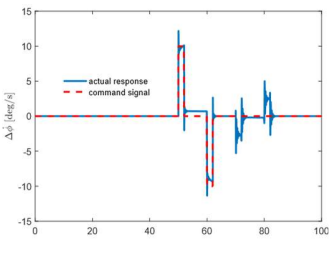

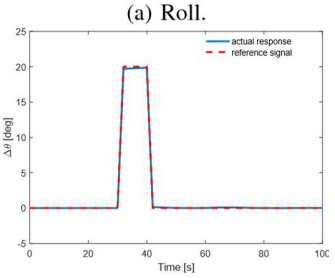

(c) Pitch.

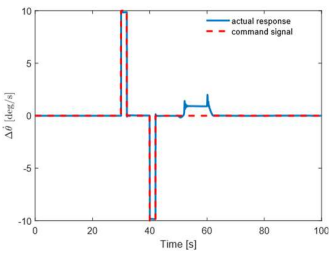

(d) Pitch rate.

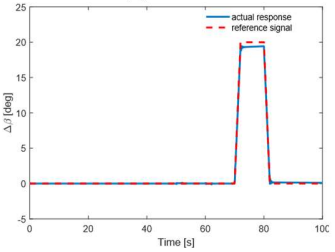

(e) Sideslip.

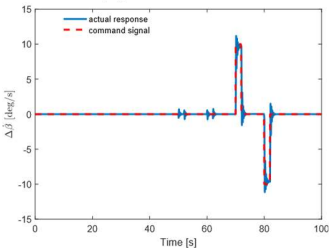

(f) Sideslip rate.

Fig. 15: Nonlinear simulation results for attitude control (airplane mode).

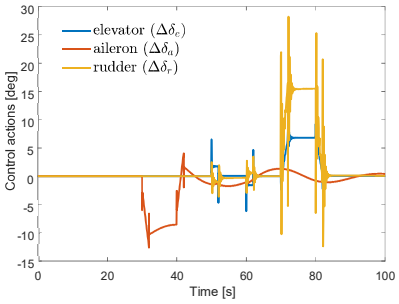

Fig. 16: Control actions (airplane mode). are recorded.

V. Conclusions

This paper exploits PID control strategy for the full flight envelope control of an eVTOL vehicle, in which 2 sets of controllers are designed specifically for 2 flight modes: helicopter mode and airplane mode. In particular, the 2 sets of controllers are able to regulate both positions/attitudes as well as their rates, making the control results more precise. The transition between these 2 modes are controlled by using DC gain scheduling, with the algorithm provided. Simulations results indicate that the control design is deemed successful,

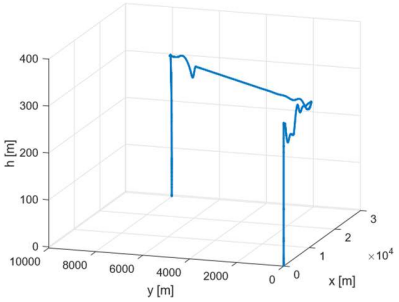

Fig. 17: Flight path (whole flight test).

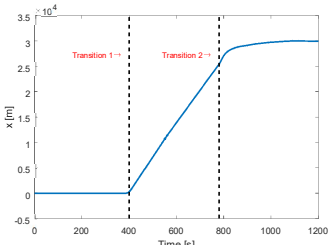

(a) Longitudinal position.

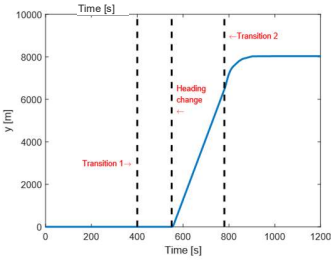

(b) Lateral position.

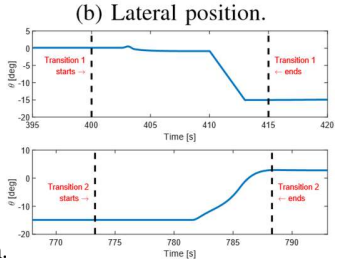

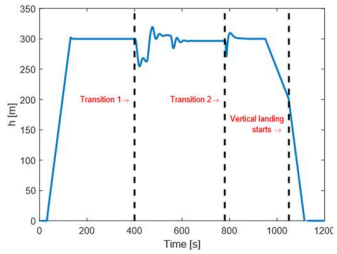

(c) Altitude.

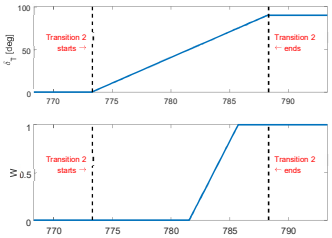

(d) Pitch attitude at 2 transition periods.

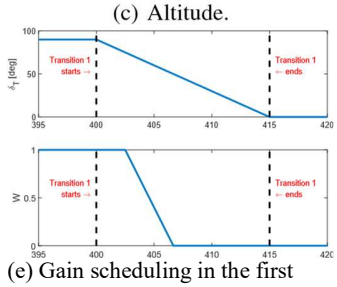

(e) Gain scheduling in the first transition.

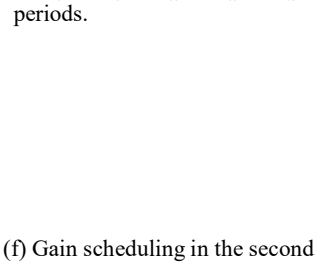

(f) Gain scheduling in the second transition.

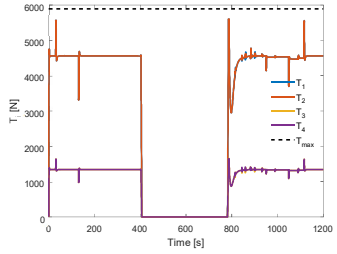

(g) Thrust.

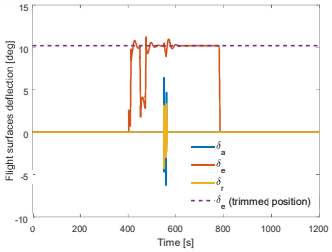

(h) Flight surfaces.

Fig. 18: Nonlinear simulation results for whole flight test.

where satisfactory performances and fast reference tracking are observed. In addition, the whole flight envelope test shows that the transition control law avoids significant altitude and attitude changes. Future work will investigate the link of the current flight control laws with higher autonomy algorithms, including trajectory planning and obstacle avoidance.

VI. Acknowledgements

This work is carried out as part of the grant MENtOR (Methods and Experiment for Novel Rotorcraft, EP/S009981/1), and the authors would like to thank Engineering and Physical Sciences Research Council (EPSRC) for their financial support. The authors are part of the UK Vertical Lift Network (UKVLN), a group of rotorcraft specialist in the UK.

References

[1] T. Lombaerts, J. Kaneshige, S. Schuet, B. L. Aponso, K. H. Shish, and G. Hardy, "Dynamic inversion based full envelope flight control for an eVTOL vehicle using a unified framework," in *Proceedings of AIAA Scitech 2020 Forum*, 2020.

[2] T. Lombaerts, J. Kaneshige, S. Schuet, B. Aponso, K. Shish, and G. Hardy, "Nonlinear dynamic inversion based attitude control for a hovering quad tiltrotor eVTOL vehicle," in *Proceedings of AIAA Scitech 2019 Forum*, 2019.

[3] Y. Song and H. Wang, "Design of flight control system for a small unmanned tilt rotor aircraft," *Chinese Journal of Aeronautics*, vol. 22, no. 3, pp. 250 – 256, 2009.

[4] J. J. Totah, "Mathematical model of a tiltwing aircraft," in *Proceedings of AIAA Scitech 1991 Forum*, 1991.

[5] R. A. Ormiston, "Revitalising advanced rotorcraft research and the compound helicopter," *The Aeronautical Journal*, vol. 120, p. 83129, 2016.

[6] G. Di Francesco and M. Mattei, "Modeling and incremental nonlinear dynamic inversion control of a novel unmanned tiltrotor," *Journal of Aircraft*, vol. 53, no. 1, pp. 73–86, 2016.

[7] I. Matamoros and C. C. de Visser, "Incremental nonlinear control allocation for a tailless aircraft with innovative control effectors," in *Proceedings of AIAA Scitech 2018 Forum*, 2018.

[8] Z. Liu, Y. He, L. Yang, and J. Han, "Control techniques of tilt rotor unmanned aerial vehicle systems: A review," *Chinese Journal of Aeronautics*, vol. 30, no. 1, pp. 135 – 148, 2017.

[9] J. Dickeson, D. Miles, O. Cifdaloz, V. Wells, and A. Rodriguez, "Robust LPV H-infinity gain-scheduled hover-to-cruise conversion for a tilt-wing rotorcraft in the presence of CG variations," in *Proceedings of the 46th IEEE Conference on Decision and Control 2007, CDC*, pp. 2773–2778, 2007.

[10] D. J. Leith and W. E. Leithead, "Survey of gain-scheduling analysis and design," *International Journal of Control*, vol. 73, no. 11, pp. 1001–1025, 2000.

[11] J. Roskam, *Airplane Flight Dynamics and Automatic Flight Controls, Part 1*. Roskam Aviation and Engineering Corporation, 1998.

[12] M. Cook, *Flight Dynamics Principles*. Elsevier, 2013.

[13] K. Alexis, G. Nikolakopoulos, and A. Tzes, "Model predictive quadrotor control: attitude, altitude and position experimental studies," *IET Control Theory Applications*, vol. 6, no. 12, pp. 1812–1827, 2012.

[14] R. Xu and mit zgner, "Sliding mode control of a class of underactuated systems," *Automatica*, vol. 44, no. 1, pp. 233 – 241, 2008.

[15] M. Efe, "Neural network assisted computationally simple $pi^{\lambda}d^{\mu}$ control of a quadrotor uav," *IEEE Transactions on Industrial Informatics*, vol. 7, no. 2, pp. 354–361, 2011.

[16] J.-J. Xiong and E.-H. Zheng, "Position and attitude tracking control for a quadrotor uav," *ISA Transactions*, vol. 53, no. 3, pp. 725 – 731, 2014.

[17] K. Lee, Y. Choi, and J. Park, "Inverse optimal design for position control of a quadrotor," *Applied Sciences*, vol. 7, p. 907, 09 2017.

[18] P. Castillo, A. Dzul, and R. Lozano, "Real-time stabilization and tracking of a four-rotor mini rotorcraft," *IEEE Transactions on Control Systems Technology*, vol. 12, no. 4, pp. 510–516, 2004.